JCBFM Open

Journal of Cerebral Blood Flow & Metabolism (2012) 32, 731–744

www.jcbfm.com

Characterisation of the contribution of the GABA-benzodiazepine α1 receptor subtype to [^{11}C]Ro15-4513 PET images

James FM Myers[1], Lula Rosso[2], Ben J Watson[1], Sue J Wilson[1,3], Nicola J Kalk[3], Nicoletta Clementi[1], David J Brooks[2], David J Nutt[3], Federico E Turkheimer[2] and Anne R Lingford-Hughes[3]

[1]*Psychopharmacology Unit, University of Bristol, Bristol, UK;* [2]*Department of Medicine, Centre for Neuroscience, Imperial College London, London, UK;* [3]*Division of Experimental Medicine, Neuropsychopharmacology Unit, Imperial College London, London, UK*

This positron emission tomography (PET) study aimed to further define selectivity of [^{11}C]Ro15-4513 binding to the GABARα5 relative to the GABARα1 benzodiazepine receptor subtype. The impact of zolpidem, a GABARα1-selective agonist, on [^{11}C]Ro15-4513, which shows selectivity for GABARα5, and the nonselective benzodiazepine ligand [^{11}C]flumazenil binding was assessed in humans. Compartmental modelling of the kinetics of [^{11}C]Ro15-4513 time-activity curves was used to describe distribution volume (V_T) differences in regions populated by different GABA receptor subtypes. Those with low α5 were best fitted by one-tissue compartment models; and those with high α5 required a more complex model. The heterogeneity between brain regions suggested spectral analysis as a more appropriate method to quantify binding as it does not *a priori* specify compartments. Spectral analysis revealed that zolpidem caused a significant V_T decrease (~10%) in [^{11}C]flumazenil, but no decrease in [^{11}C]Ro15-4513 binding. Further analysis of [^{11}C]Ro15-4513 kinetics revealed additional frequency components present in regions containing both α1 and α5 subtypes compared with those containing only α1. Zolpidem reduced one component (mean ± s.d.: 71% ± 41%), presumed to reflect α1-subtype binding, but not another (13% ± 22%), presumed to reflect α5. The proposed method for [^{11}C]Ro15-4513 analysis may allow more accurate selective binding assays and estimation of drug occupancy for other nonselective ligands.
Journal of Cerebral Blood Flow & Metabolism (2012) **32,** 731–744; doi:10.1038/jcbfm.2011.177; published online 4 January 2012

Keywords: GABA; imaging; kinetic modelling; pharmacokinetics; positron emission tomography

Introduction

Imaging studies of benzodiazepine receptors over the past 20 years have revealed different levels of binding in patients with anxiety and panic disorders, alcoholism, schizophrenia, epilepsy, and other disorders (Malizia *et al*, 1998; Lingford-Hughes *et al*, 2010; Busatto *et al*, 1997; Hammers *et al*, 2001). There is increasing knowledge about the six different subtypes of the GABA-benzodiazepine receptor, their locations in the brain, and their functional implications. For instance, knock-in and knockout genetic manipulations in mice have shown that the GABA-benzodiazepine receptor subtype containing the α1 subtype is important in sedation and sleep, the α2/3 subtype is involved in anxiety, and the α5 in learning and memory (Möhler *et al*, 2002). In the light of these discoveries, it is important to study the role of these receptor subtypes in humans. Neuroimaging, in particular positron emission tomography (PET) and single-photon emission tomography (SPET) imaging with receptor-selective ligands, remains the only way of quantifying benzodiazepine receptors in the human brain *in vivo*.

[^{11}C]flumazenil with PET is the most commonly used *in vivo* marker of benzodiazepine receptor binding and its iodinated analogue, [^{123}I]iomazenil, can be used with SPET. Flumazenil is an antagonist that binds with high affinity to benzodiazepine receptors of the α1, α2, α3, or α5 (Ki ~1 nmol/L)

Correspondence: Professor AR Lingford-Hughes, Division of Experimental Medicine, Neuropsychopharmacology Unit, Imperial College, Burlington Danes Building, Hammersmith Hospital Site, 160 Du Cane Road, London W12 0NN, UK.
E-mail: anne.lingford-hughes@ic.ac.uk
This study was supported by MRC Programme Grant (G0400575), UK Medical Research Council PET Methodology Programme Grant, and MRC/University of Bristol PhD studentship (JFM).
Received 27 April 2011; revised 16 September 2011; accepted 12 October 2011; published online 4 January 2012

subtypes and with lower affinity to the α4 or α6 subtypes (Ki ~150 nmol/L (Sieghart, 1995)). Until recently, there was no way of preferentially visualising particular subtypes. Ro15-4513 shows 10- to 15-fold selectivity for the α5 subtype over others *in vitro* (Ki 0.07 nmol/L versus 1 to 5 nmol/L), and *in vivo* [11C]Ro15-4513 PET provides a relatively selective marker for the GABARα5 subtype (Hadingham *et al*, 1993; Lingford-Hughes *et al*, 2002; Maeda *et al*, 2003). These studies, among others, show that *in vivo* [11C]Ro15-4513 uptake targets the limbic system, with the anterior cingulate cortex, ventral striatum, and hippocampus showing particularly high levels (Onoe *et al*, 1996), whereas high [11C]flumazenil binding is seen in all cortical areas, with highest levels in the occipital cortex. Therefore, the limbic pattern of [11C]Ro15-4513 binding is likely to be relevant to learning, memory, reward, and addiction. For example, we have shown that an inverse agonist at the α5 subtype can reverse the memory-impairing effects of acute alcohol consumption (Nutt *et al*, 2007), and [11C]Ro15-4513 binding is related to performance on a verbal memory task in alcohol dependence (Lingford-Hughes *et al*, 2010). The α5 subtype has also been implicated in the reinforcing effects of alcohol in mice (Stephens *et al*, 2005), and we have shown a reduction in [11C]Ro15-4513 binding in the nucleus accumbens in alcohol dependence compared with healthy controls (Lingford-Hughes *et al*, 2010).

Although the distribution of [11C]Ro15-4513 binding is consistent with relatively greater labelling of the α5 subtype, the affinity of [11C]Ro15-4513 is only an order of magnitude greater for the α5 over other subtypes. Given the abundance of the α1 subtype throughout the brain, it is important to assess the contribution of α1 binding to [11C]Ro15-4513 binding. This study compares the binding of [11C]Ro15-4513 with that of [11C]flumazenil in the presence and absence of zolpidem, a compound with selectivity for the α1 receptor subtype that is >5,000-fold over that for the α5 subtype (Hanson *et al*, 2008; Langer *et al*, 1992). Unlike classical benzodiazepines, the sedative/hypnotic effect of zolpidem occurs at much lower doses than the other pharmacological effects attributed to benzodiazepine-site action, such as anticonvulsant activity and muscle relaxation (Sanger, 2004).

After predosing with zolpidem or placebo, one group of healthy volunteers was scanned with [11C]Ro15-4513 and another group with [11C]flumazenil. Our hypothesis was that, because [11C]flumazenil labels the α1 subtype, its binding would be reduced by zolpidem. In contrast, we hypothesised that [11C]Ro15-4513 binding would not be altered by zolpidem in α5-rich regions such as the hippocampus, whereas in α1-rich regions with limited or no α5, such as the cerebral cortex and thalamus, [11C]Ro15-4513 binding might be reduced. To further resolve contributions of α1 and α5 subtypes to the [11C]Ro15-4513 signal, we applied spectral analysis (Cunningham and Jones, 1993) to both [11C]Ro15-4513 and [11C]flumazenil data sets to deduce the spectral band of the GABA-benzodiazepine α1 subtype. The range obtained was used to determine the occupancy by zolpidem of the GABA α1 subtype from the [11C]Ro15-4513 data using the Lassen plot (Lassen *et al*, 1995; Cunningham *et al*, 2010).

Materials and methods

This study was approved by a NHS Research Ethics Committee, the Administration of Radioactive Substances Advisory Committee and local NHS Research and Development. It was conducted in accordance with Good Clinical Practice—International Conference on Harmonisation guidelines.

Design

There were two separate randomised double-blind placebo-controlled studies, each with six healthy volunteer participants. The study procedures were identical apart from the PET ligand used: [11C]flumazenil for one study and [11C]Ro15-4513 for the other. Positron emission tomography scans were performed twice for each participant, once after zolpidem and once after placebo, with at least a week between scans. Binding of the ligand was compared between the two conditions.

Subjects

Healthy male volunteers (age mean ± s.d.: [11C]Ro15-4513: 44 ± 6 years; [11C]flumazenil: 43 ± 4 years) underwent 2 PET scans at least a week apart, after zolpidem or placebo, the order of which was randomised. They were all screened with urinalysis for illicit drugs of abuse, had no current or previous significant physical or mental disorders, had taken no psychotropic drugs in the last month, nor were regular benzodiazepine users.

Zolpidem and Measures

Zolpidem (20 mg) or an identical placebo was administered 90 minutes before radioligand injection and at the start of the PET scan. Plasma zolpidem levels were measured at the time of PET ligand injection.

The following tasks provided a measure of the effect of zolpidem on brain function. Saccadic eye movements to a target were measured using electrooculography as described previously (Lingford-Hughes *et al*, 2005). The subject was asked to fixate on a red light as it appeared on the screen mounted 67 cm in front of him. Data were then collected for 48 eye movements of 15° to 40° and a main sequence curve obtained, the measurement for peak velocity being the interpolation at 35°. Verbal memory was tested with learning and delayed recall of a list of 20 words (Nutt *et al*, 2007), with the list presented at the start of the scan and recall 30 minutes later.

Positron Emission Tomography Method

[11C]Ro15-4513 was synthesised by *N*-methylation of the *N*-desmethyl derivative with [11C]iodomethane. Reverse-phase high-performance liquid chromatography was used to purify the compound (Phenomenex Ultra-carb 7 ODS, $250 \times 10\,mm^2$). [11C]flumazenil was synthesised by methylation of the nor-derivative with $^{11}CH_3I$.

A bolus injection of [11C]flumazenil (mean ± s.d.: 476 ± 11 MBq in 1.0 ± 0.16 mL) or [11C]Ro15-4513 (mean ± s.d.: 495 ± 18 MBq in 3.3 ± 0.49 mL) was administered through an intravenous cannula sited in the dominant antecubital fossa vein. No significant differences in cold mass injected, with paired *t*-tests, between placebo and zolpidem scans were found using either flumazenil (mean ± s.d.: 1.37 ± 0.52 μg to 1.09 ± 0.28 μg, $t = 1.28$, $P > 0.25$) or [11C]Ro15-4513 (mean ± s.d.: 3.22 ± 0.86 μg to 4.30 ± 3.71 μg, $t = 0.579$, $P > 0.5$).

We used a Siemens ECAT EXACT HR+ (CTI/Siemens, model 962; Knoxville, TN, USA) scanner with an axial field of view of 15.5 cm. Subjects were positioned such that the transaxial images were parallel to the intercommissural line. A total of 63 transaxial image planes were acquired as 2.42-mm slices with a reconstructed axial resolution of 5.4 mm and a transaxial resolution of 5.6 mm (Spinks *et al*, 2000). A 10-minute transmission scan was acquired before every emission using a single rotating photon point source of ^{137}Cs for subsequent attenuation and scatter correction.

[11C]Ro15-4513 scans comprised 24 dynamic time frames (1×30, 4×15, 4×60, 2×150, 10×300, 3×600 seconds) and [11C]flumazenil scans comprised 20 time frames (1×30, 4×15, 4×60, 2×150, 2×300, 7×600 seconds) of data which, after corrections for attenuation, random coincidences, and scatter, were all reconstructed using filtered backprojection. The three-dimensional emission data were Fourier-rebinned (Defrise *et al*, 1997) into two-dimensional data sets to increase the speed of reconstruction.

Each subject had a radial arterial cannula inserted in the nondominant wrist to allow continuous counting of blood radioactivity concentration for the first 15 minutes of the experiment using a bismuth germanate counter. Discrete samples were also taken 4, 6, 8, 10, 20, 35, 50, 65, 80, and 90 minutes after injection. An aliquot of each discrete sample was rapidly centrifuged to obtain corresponding plasma and radioactivity concentrations. The continuous blood counts were corrected using the estimated plasma/blood ratio to derive the plasma radioactivity profile. The plasma was further analysed for radiolabelled metabolites using a semiautomated analysis system, consisting of an on-line solid-phase sample enrichment column and high-performance liquid chromatography. The amount of [11C]Ro15-4513 or [11C]flumazenil in the plasma at a given time point was calculated as a percentage of all radioactive components separated by high-performance liquid chromatography added to the radioactivity present in the solid-phase extraction fraction, to produce a final plasma input function derived for radioligand-binding quantification. These calculations were carried out using Clickfit, in-house software running in Matlab (The Mathworks, Natick, MA, USA).

All subjects had T1-weighted magnetic resonance imaging with a Philips 1.5-T Gyroscan Intera scanner (Philips, Best, The Netherlands) to produce structural images for reference.

Image and Blood Analysis

Reconstructed PET images were analysed on a Sun SPARC workstation (Sun Microsystems, Mountain View, CA, USA) using Analyze AVW version 8.1 (Biomedical Imaging Resource, Mayo Clinic, Rochester, MN, USA), Matlab 6 and 6.5 (The Mathworks), and SPM5 (available through http://www.fil.ion.ucl.ac.uk/spm/; FIL, 12 Queen Square, London, UK).

Regions of interest were placed on the images using a probabilistic map which defined 83 regions (Hammers *et al*, 2007). A list of these regions is given in Appendix 1. Each structural magnetic resonance image was coregistered to the PET add image, a sum of all counts acquired during the scan, using a rigid-body technique. This coregistered magnetic resonance imaging was then normalised to the 'Montreal Neurological Institute' space (International Consortium for Brain Mapping (ICBM)/MNI) using a bias-corrected segmentation in SPM5. Using the reverse parameters of this normalisation, the probabilistic map could be warped to fit the coregistered structural magnetic resonance imaging and hence the add image and the original PET dynamic. The goodness of fit of each object map to the individual brain was checked visually before regional sampling using the region of interest tool in Analyze 8.1. From the probabilistic map, we identified regions with wide differences in α1 and α5 distribution: the cerebellum, occipital cortex, and thalamus, which contain high α1 levels and very low α5 levels, and limbic regions such as the hippocampus, nucleus accumbens, amygdala, and anterior cingulate cortex with high α5 levels and lower α1 levels (Fritschy and Möhler, 1995; Lingford-Hughes *et al*, 2002).

Modelling

Parametric maps of total volume of distribution (V_T) were created for both [11C]Ro15-4513 and [11C]flumazenil images using receptor parametric mapping software written in Matlab (RPM, MRCCU (Cunningham and Jones, 1993)). Values for mean V_T per voxel in each region of interest and in combined regions were then sampled in Analyze 8.1, to compare *in vivo* binding with and without zolpidem, for the two different PET ligands.

The regional kinetics of uptake of [11C]Ro15-4513 only were computed from brain and plasma time-activity curves (TACs) using one-tissue and two-tissue compartment models, using Clickfit. Having estimated the delay, the models used fixed blood volume (V_b) of 0.06, calculated after a preliminary analysis of variable V_b and averaged over 83 regions of interest. Goodness of fit for each model in every region was represented using Akaike information criteria. V_T of [11C]Ro15-4513 was then calculated from the estimation of kinetic parameters in the two models using the following equations: one-tissue compartment $V_T = K_1/k_2$; two-tissue compartment $V_T = \frac{K_1}{k_2}\left(1 + \frac{k_3}{k_4}\right)$.

Spectral Analysis

To further elucidate the pharmacokinetics of [11C]Ro15-4513, Clickfit was again used to carry out spectral analysis of each regional TAC collected from the original PET dynamics. Spectral analysis (Cunningham and Jones, 1993; Turkheimer *et al*, 1994) convolves the arterially derived metabolite-corrected plasma input function with a first-order poly-exponential, without specifying the number of tissue compartments, to fit the TAC for any region, under the assumptions of system linearity and time invariance. The impulse response function (IRF) is described as $\mathrm{IRF}(t) = \sum_i \alpha_i e^{\beta_i t}$, where α and β are real, nonnegative numbers. Overall, 100 discrete values of β on a logarithmic scale (Turkheimer *et al*, 1994), corresponding to 100 different basis functions, were chosen, between 0.000631 to 1.0 seconds^{-1}, a lower limit shown to show the greatest interclass correlation coefficient (Barros *et al*, 2010). The 'spectrum' of peaks with height α, can be used to infer pharmacological characteristics of the ligand and its binding properties. Given that the area under the IRF function is the total volume of distribution, the position and height of spectral peaks can be used to estimate V_T using $V_\mathrm{T} = \sum_{k=i}^{n} (\alpha_k/\beta_k - \lambda)$, where n is the total number of peaks, α_k the kth peak height, β_k is kth peak position, and λ the decay constant.

In the case of two specific binding sites, the total volume of distribution V_T can be written as $V_\mathrm{T} = V_{S1} + V_{S2} + V_\mathrm{ND}$, the sum of the specific distribution volumes, V_{S1} and V_{S2}, and the nondisplaceable distribution volume V_ND. Particularly, for [11C]Ro15-4513, the V_{S1} relative to the specific binding to GABARα5 and V_{S2} relative to the specific binding to GABARα1 may be determined comparing the contribution of different kinetics to the IRF in α5-rich regions with those in region with little or no α5 density, before and after blocking of the α1-binding signal by zolpidem. As the IRF is linear, V_S may be estimated for particular regions of the spectrum, $V_S = \sum_{k=i}^{j} (\alpha_k/\beta_k - \lambda)$, where i and j are integers, $j > i$, representing β-values defined by pharmacological and regional inference. The ranges of β chosen to estimate V_S for different subtypes are described in detail in the 'Results' section. All peaks with $\beta > 0.001$ seconds^{-1} were, attributed to their fast curve shape, assumed to represent blood volume and nonspecific binding, and were therefore excluded with a low-pass filter. A similar band-pass approach to spectral analysis, based on regionally informed frequency allocation, has been used to investigate cerebral protein synthesis using L-[1-11C]leucine PET by Veronese *et al,* (2010).

Occupancy Plots

Occupancy data were derived graphically, as described by Lassen *et al* (1995) (Cunningham *et al*, 2010), using the vectors of the regional volumes of distribution in baseline, $\mathbf{V}_\mathrm{T}^b$, and postdrug, $\mathbf{V}_\mathrm{T}^d$, as follows: $\mathbf{V}_T^b - \mathbf{V}_T^d = \mathrm{O}^d$ $(\mathbf{V}_T^b - V_\mathrm{ND})$, assuming that the V_ND and O^d, the receptor occupancy of the blocking drug, were constant across brain regions.

If the imaging ligand has two binding sites and the blocking drug is selective for only one of these binding sites, $\mathbf{V}_\mathrm{T}^b$ and $\mathbf{V}_\mathrm{T}^d$ may be written as follows:

$$\begin{aligned} \mathbf{V}_T^b &= \mathbf{V}_{S1}^b + \mathbf{V}_{S2}^b + V_{ND} \\ \mathbf{V}_T^d &= \mathbf{V}_{S1}^d + \mathbf{V}_{S2}^d + V_{ND} = \mathbf{V}_{S1}^b + \mathbf{V}_{S2}^b(1 - \mathrm{O}^d) + V_{ND} \end{aligned} \quad (1)$$

Therefore, we can draw two plots for the fractional volumes of distribution defined above:

$$\begin{aligned} \mathbf{V}_{S1}^b - \mathbf{V}_{S1}^d &= 0 \\ \mathbf{V}_{S2}^b - \mathbf{V}_{S2}^d &= \mathrm{O}^d \mathbf{V}_{S2}^b \end{aligned} \quad (2)$$

The specific volume of distribution of [11C]Ro15-4513 relative to each subtype was derived using spectral analysis with the assumption that a given spectral range corresponded to binding to a single site. In addition, we made the further assumption that, although the blocking drug will change the positions of the spectral peaks, the volume of distribution of the imaging ligand relative to the binding to the site not targeted by the cold drug will be the same in the baseline and postdrug PET studies. Both assumptions were tested using zolpidem blocking data, as reported in the 'Results' section. The 83 region atlas (Appendix 1) provided a large number of regional volumes of distributions for use in the plots. The gradient of a linear regression through the points on the axes, $x = (V_\mathrm{S}^b)$, $y = (V_\mathrm{S}^b - V_\mathrm{S}^d)$, estimated the zolpidem occupancy O^d at the given receptor subtype.

Statistical Analysis

Two-tailed Student's *t*-statistic was used to interrogate demographic variables, zolpidem levels, as well as objective and subjective measures between the two scanning groups and within groups in the presence and absence of zolpidem. Mean V_T estimates for the whole brain with and without zolpidem were also compared with Student's *t*-test, whereas the effect of zolpidem on binding in selected regions (such as the whole brain, occipital cortex, cerebellum, hippocampus, nucleus accumbens, frontal lobe, anterior cingulate, amygdala), was interrogated with two-way analysis of variance (ANOVA). Two-way repeated-measures ANOVA with P-plot graphical test and the Hochberg multiple comparison correction (Turkheimer *et al*, 2001) across all 83 regions was used to compare [11C]Ro15-4513 and [11C]flumazenil V_T, with and without zolpidem. One-way ANOVA was used to compare the estimated parameters of the different compartmental models, with pairwise comparisons conducted using Tukey's *post hoc* tests. To test the significance of the line through the regional V_T estimates in occupancy plots, linear regressions were used. All statistical analyses were conducted using GraphPad Prism (version 4.02 for Windows, GraphPad Software, San Diego, CA, USA, http://www.graphpad.com).

Results

One [11C]Ro15-4513 pair of scans was not analysable after a subject dropped out of the study, so we report here the remaining five. There was no significant difference in zolpidem levels in the two groups, although only three blood samples were successfully acquired in the [11C]Ro15-4513 cohort (mean ± s.d.:

[11C]Ro15-4513 $n=3$: 107.9 ± 33.1 ng/mL; [11C]flumazenil $n=6$: 84.9 ± 41.1 ng/mL; $t=0.84$; $P>0.40$). These levels are consistent with those reported in the literature (Salvà and Costa, 1995). Zolpidem resulted in impaired saccadic eye movements: peak velocity at 90 minutes postingestion was 11.9% after placebo and 38.1% after zolpidem ($t=3.75$; $P<0.005$); the percentage of failed saccades was 20.3% after placebo and 59.4% after zolpidem ($t=4.60$; $P<0.0005$). Zolpidem also impaired learning and delayed recall of the 20-word list similarly in both groups. In the [11C]Ro15-4513 group, the number of words recalled reduced from 6.8 ± 4.2 to 3.4 ± 4.0 and in the [11C]flumazenil group from 9.2 ± 5.1 to 2.2 ± 1.7.

Compartmental Modelling of [11C]Ro15-4513

Compartmental modelling was applied to all [11C]Ro15-4513 regional data, estimating kinetic parameters and goodness of fit, represented by the Akaike information criteria. All data for the placebo group are shown in Table 1, presented as mean ± s.d. for both models. All rate constants are expressed as seconds^{-1}.

Using a one-tissue compartment model with fixed V_b (2kbvf), estimates of $K1$ and $k2$ were consistently small and positive, through all regions and all individuals ($K1 = 0.0050 \pm 0.0011$; $k2 = 0.0015 \pm 0.0008$). V_b was fixed at 0.06, calculated as the average of estimated V_b in all 83 regions.

The two-tissue compartment model (4kbvf), yielded, on average, higher estimates for $K1$ and $k2$ than did the one-tissue compartment model, but very low values for both $k3$ and $k4$, expressed as seconds^{-1} (4kbvf results: $K1 = 0.0053 \pm 0.0001$; $k2 = 0.0019 \pm 0.0001$; $k3 = 0.00042 \pm 0.00443$; $k4 = 0.00050 \pm 0.00731$). These differences were statistically significant applying a one-way ANOVA for each model parameter. Mean estimations of $K1$ and $k2$ from the four different models were significantly different ($K1$: $F=13.71$; $P<0.0005$, $k2$: $F=12.49$; $P<0.0005$), and Tukey's *post hoc* tests showed significance for both $K1$ and $k2$ ($P<0.01$) in all comparisons of one- to two-tissue models.

Kinetic modelling of TACs from regions rich in GABARα1 receptors gave differing results compared with regions rich in GABARα5 receptors. In the GABARα1-rich cerebellum, the one-tissue compartment model fitted TACs almost as well as did the two-tissue compartment model (Akaike information criteria better in 3 of 5 individuals, average 6.8% more negative), but the two-tissue model produced consistently very small negative estimates of either or both $k3$ and $k4$. However, in the GABARα5-rich hippocampus, there was a significantly better fit using the two-tissue model compared with the one-tissue model (Akaike information criteria better in all individuals, average 46.9% more negative) and estimates of BP (calculated using k_3/k_4) that were positive and small.

Although the estimates of rate constants differed significantly, as did the fits of the curves, similar overall V_Ts were obtained with each model, and both models showed the same pattern of variability between individuals.

Table 1 Comparison of the kinetic rate constants obtained using different compartmental models to determine Ro15-4513 binding in the brain

	K1	*k2*	*k3*	*k4*	*AIC*
All regions					
2kbvf	5.0 ± 1.1	1.5 ± 0.8	—	—	−89.09 ± 27.8
4kbvf	5.4 ± 1.1	1.9 ± 1.2	0.42 ± 4.43	0.50 ± 7.31	−100.76 ± 28.8
Cerebellum					
2kbvf	6.0 ± 0.7	3.1 ± 0.4	—	—	−126.43 ± 18.1
4kbvf	NA	NA	NA	NA	NA
Hippocampus					
2kbvf	4.3 ± 0.4	0.77 ± 0.13	—	—	−63.46 ± 13.6
4kbvf	5.2 ± 0.5	1.6 ± 0.5	0.75 ± 0.56	0.48 ± 0.81	−93.79 ± 15.6

AIC, Akaike information criteria; NA, not available.
All constants are expressed as mean ± s.d. secconds × 10^{-3}. Binding in the cerebellum was not successfully evaluated by a two-tissue compartment model.

Spectral Analysis

[11C]Ro15-4513: As previously reported, the highest [11C]Ro15-4513 V_Ts were seen in limbic regions such as the nucleus accumbens and hippocampus (see Figure 1A; Lingford-Hughes *et al* (2002, 2010)). All results are presented as mean ± s.d. There was no reduction in [11C]Ro15-4513 V_T in the presence of zolpidem in the whole brain (postplacebo: 3.69 ± 0.22; postzolpidem: 3.81 ± 0.47) nor among the combined regions ($F=0.0107$; $P>0.90$; see Figure 1B). Sampling all of the 83 regions from the probabilistic map, a repeated-measures ANOVA showed a marginally significant increase in V_T ($F=4.363$; $P<0.05$) after zolpidem. There was some variation between individuals (see Figure 1), with zolpidem causing a reduction in binding in one subject.

[11C]Flumazenil: For [11C]flumazenil binding, a significant effect of zolpidem was observed. Throughout the whole brain, V_T was ~10% lower in the presence of zolpidem (V_T postplacebo: 4.10 ± 0.56; postzolpidem: 3.70 ± 0.37; $F=14.57$; $P<0.0005$; see Figure 2). The effect remained significant when all 83 regions were sampled ($F=123.7$; $P<0.0001$). No individual region survived correction for multiple comparisons. Zolpidem reduced [11C]flumazenil V_T in four of the six volunteers (see Figure 2B).

Spectral Analysis: Assessment of Spectral Peaks

The distribution of spectral peaks in different regions was identified using Clickfit. Each region yielded a

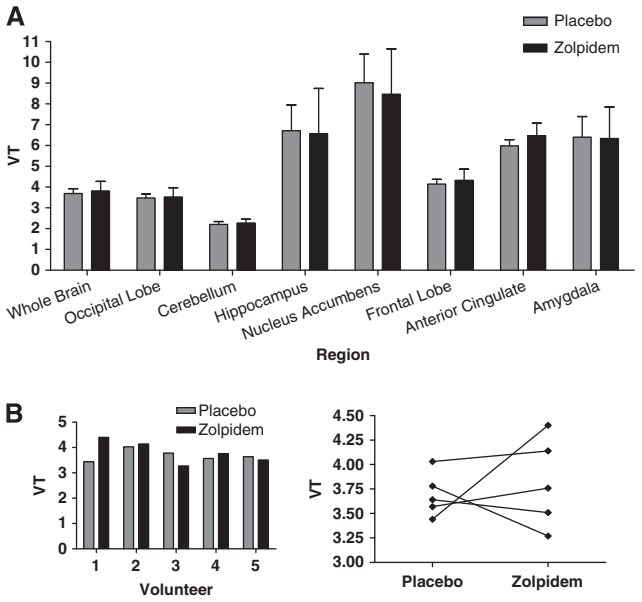

Figure 1 [11C]Ro15-4513 scans. (**A**) Estimates of mean [11C]Ro15-4513 V_T in different ROIs with and without zolpidem. Error bars show s.e.m. of the five volunteers. (**B**) Intersubject variability, for the five volunteers, in [11C]Ro15-4513 V_T estimation in the whole brain. These data represent similar trends for each ROI within the subjects. ROI, region of interest.

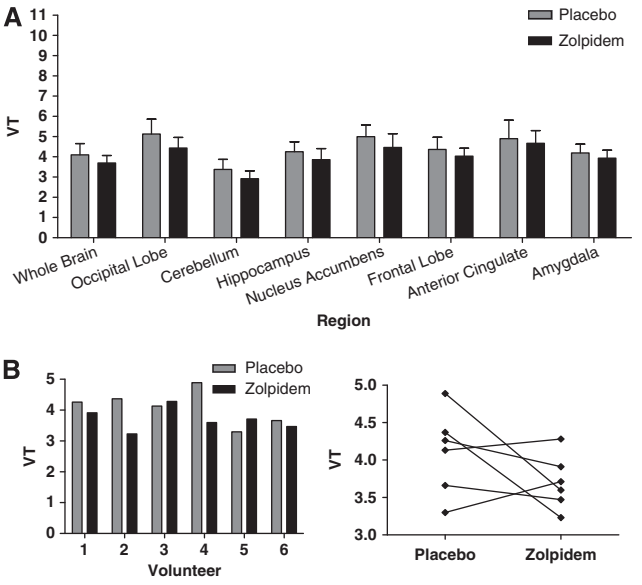

Figure 2 [11C]Flumazenil scans. (**A**) Estimates of mean flumazenil V_T in different ROIs with and without zolpidem. Error bars show s.e.m. of the six volunteers. In each region, there is an observable decrease in binding with zolpidem administration, although significance did not survive *post hoc* correction. Significant trends were seen using a two-way ANOVA, with these combined regions, and all subregions in the whole brain. (**B**) Intersubject variability, for the six volunteers, in [11C]flumazenil V_T estimation in the whole brain. These data represent similar trends for every individual region, and more consistent decreases than for [11C]Ro15-4513 lead to a more significant overall trend. ANOVA, analysis of variance; ROI, region of interest.

different spectrum of peaks, each peak position representing one of 100 values of β, described in the 'Materials and methods' section. These results were pooled and a summed peak height for each peak was calculated for each region and each PET tracer in the presence or absence of zolpidem. The average height for each β-value was not representative of the true peak distribution, because the peaks are discrete and the spectral analysis algorithms assign consecutive values for those peaks not matching a predefined β.

There was a clear average peak height decrease with zolpidem for both ligands. For [11C]Ro15-4513, the differences were seen between 0.0020 and 0.0030 seconds^{-1}. With [11C]flumazenil, the decreases were seen at faster rates, between 0.0030 and 0.0050 seconds^{-1} (data not shown).

To further investigate the source of these differences, a smaller number of brain regions with high and low α1 levels were selected for further analysis. Figures 3 and 4 illustrate data for the cerebellum and hippocampus after [11C]Ro15-4513 and [11C]flumazenil, respectively. As zolpidem is a GABARα1 agonist, it was expected that regions with high α1 levels and low levels of other GABA receptor subtypes should show a greater change in peak profile than areas with lower α1 levels. In the cerebellum, a region with almost solely high α1 levels, the fast kinetic profile for [11C]Ro15-4513 without zolpidem represents α1 subtype binding (average height = 0.00306 seconds^{-1}; range of peaks 0.0030 to 0.0040 seconds^{-1}, see Figure 3A). Zolpidem reduced average [11C]Ro15-4513 peak height, lessening the contribution of those curves to the IRF and spreading their range (average height = 0.00185 seconds^{-1}; range of peaks 0.0020 to 0.0060 seconds^{-1}, Figure 3A). The effect of zolpidem was estimated for this band of peaks in the cerebellum, to assess proposed α1 blockade. There was a significant decrease in V_S after zolpidem (3.99 ± 0.31 to 3.41 ± 0.22, $t = 2.827$; $P < 0.05$).

In contrast, in the hippocampus, a region with high α5 levels but also containing the α1 subtype, there are two clear ranges of kinetic components of [11C]Ro15-4513 (see Figure 3B). The fast component in the placebo scan (average height = 0.00122 seconds^{-1}; range of peaks 0.0025 to 0.0045 seconds^{-1}) is reduced and broadened in the presence of zolpidem (average height = 0.00065 seconds^{-1}; range of peaks 0.0020 to 0.0060 seconds^{-1}). This reduction in V_S is significant (1.40 ± 0.92 to 0.44 ± 0.60, $t = 2.369$; $P < 0.05$) and analogous to that found in the cerebellum, suggesting that this peak range reflected the α1 subtype. In the hippocampus, there was also a slower component, unaffected by zolpidem (11.51 ± 3.44 to 10.00 ± 2.59, $t = 0.8291$; $P > 0.45$), which contributed to the majority of the convolution after zolpidem administration (placebo: average height = 0.00179 seconds^{-1}; range

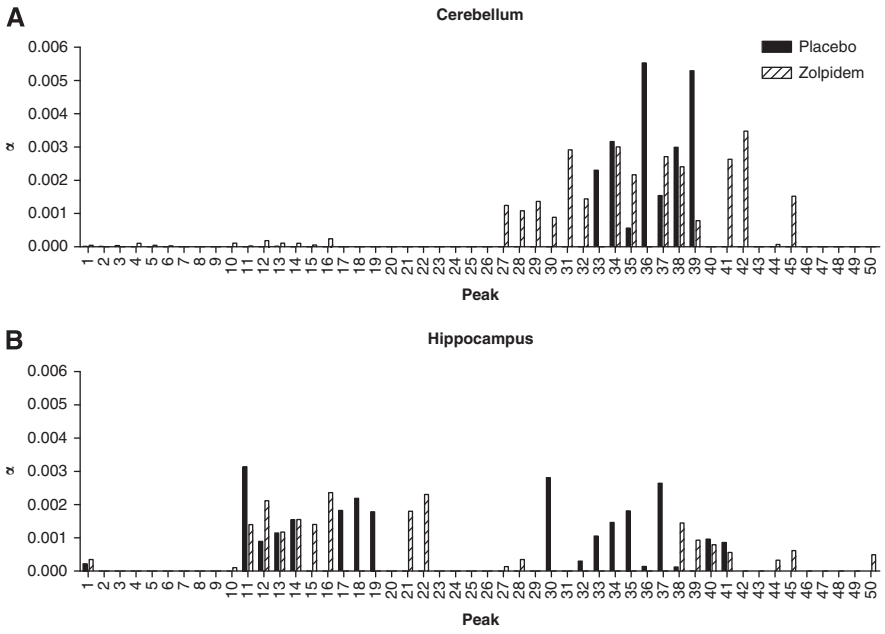

Figure 3 Comparison of [11C]Ro15-4513 spectral analysis results in (**A**) the cerebellum and (**B**) hippocampus, with data summed over five subjects. Only peaks 1 to 50 (frequency range 0.000631 to 0.00873 seconds^{-1}) are shown.

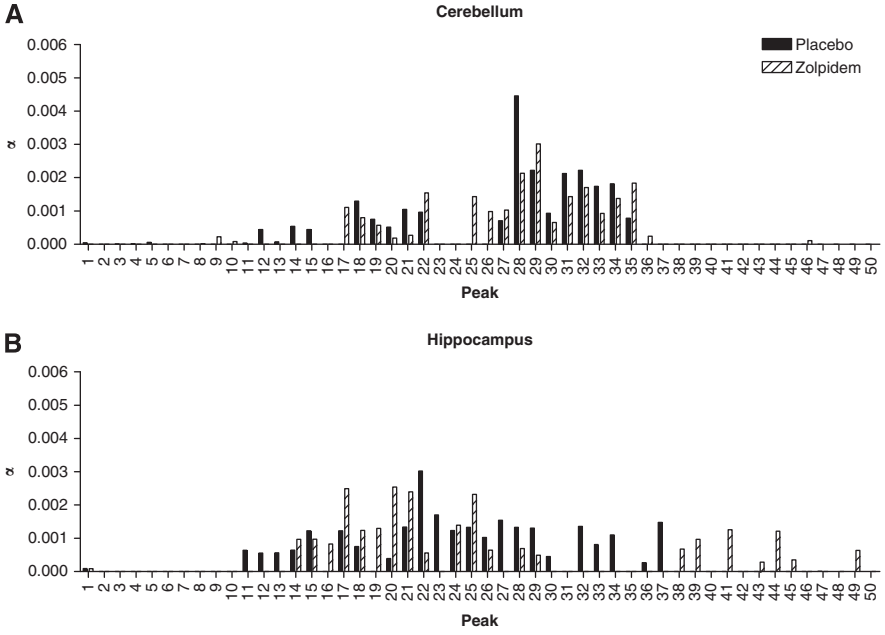

Figure 4 Comparison of [11C]flumazenil spectral analysis results in (**A**) the cerebellum and (**B**) hippocampus with data summed over five subjects. Only peaks 1 to 50 (frequency range 0.000631 to 0.00873 seconds^{-1}) are shown.

of peaks 0.0010 to 0.0014 seconds^{-1}; zolpidem: average height = 0.00177 seconds^{-1}; range of peaks 0.0010 to 0.0016 seconds^{-1}, Figure 3B).

Comparable results for spectral analysis of [11C]flumazenil in the cerebellum and hippocampus are shown in Figure 4. Although there are no clear distinctions between fast and slow kinetic components, there are differences in estimates of V_T. For peaks between 10 and 50, there is a consistent and trend-level decrease in binding after zolpidem administration in the cerebellum (6.11 ± 1.18 to 5.16 ± 0.42, $t = 3.343$; $P < 0.06$), and significant in the hippocampus (7.78 ± 0.98 to 6.40 ± 1.37, $t = 2.923$; $P < 0.05$). The homogeneity of the spectra precluded any further separation of peaks based on regional receptor densities.

Occupancy Estimation

The lack of effect on average V_S by zolpidem in the 'slower' end of the spectrum, and the decrease in the 'faster' range, led to broad estimates of i and j that would include all peaks in the two ranges. V_S values were calculated for both slow range ($i=1$; $j=25$) and fast ($i=25$; $j=50$), with and without zolpidem. (V_S^b) was plotted against ($V_S^b - V_S^d$) to produce occupancy plots, shown in Figure 5. For the slow range, little or no occupancy was shown, as expected because this was assumed to represent binding to the α5 subtype (Figure 5A). Two of the five regression plots were significantly different from zero, but with values of occupancy $<20\%$, one positive and one negative. For the fast range, representing the α1 subtype, there are positive estimates of occupancy between 42.9 and 84.8% (mean ± s.d.: 64.3% ± 15.2%), with linear regression significantly different from 0 consistently with $P<0.0001$ (Figure 5B).

Occupancy was also estimated using plots for each of the six volunteers in the [11C]flumazenil cohort. The results are shown in Figure 6. V_T was calculated by voxel-wise spectral analysis described earlier. Only 2 volunteers showed data fitted significantly by regression, giving zolpidem occupancy estimates of 30 and 33%.

Discussion

We have shown that zolpidem significantly reduced [11C]flumazenil V_T in the whole brain by ∼10%, whereas there is no reduction in [11C]Ro15-4513 V_T. These results suggest that the GABARα1 binding of [11C]Ro15-4513 does not significantly affect overall V_T, whether estimated by spectral analysis to produce parametric maps of V_T, or by compartmental modelling. However when frequency components of spectra derived from [11C]Ro15-4513 images, proposed to reflect binding to the α1 subtype, are used to estimate V_S, occupancy by zolpidem is shown to range from 43% to 85%. The dose of zolpidem was shown to be clinically relevant as it induced sedation and significantly impaired saccadic eye movement performance and word list recall.

The difference in binding properties of nonselective ligands in regions with differing populations of receptor subtypes ought to be demonstrable by applying various compartmental models. We hypothesised that more complex models would be required where there are multiple subtypes compared with brain regions with predominantly one subtype. One- and two-tissue compartmental models showed similar variability between individuals, but a different quality of fit to the data depending on region. In the cerebellum, an α1-rich region, one-tissue compartment models provided the best fit for observed data, with higher K_1 and k_2. Pharmacologically, this corresponds to the rapid kinetic profile expected from the fast binding of a benzodiazepine ligand with relatively low affinity to the cerebellar subtypes. By contrast, in the hippocampus, the two-tissue compartment model was superior to the one-tissue compartment model. In addition, lower estimates of k_2 suggested a slower kinetic profile to that in the cerebellum. We suggest that this slower kinetic profile represents high-affinity binding to the GABARα5 subtype in α5-rich regions. These results are consistent with those of Maeda *et al* (2003) in nonhuman primates, who also showed that there are different kinetic components in regions containing different subtype levels and ratios.

Both [11C]flumazenil and [11C]Ro15-4513 bind to more than one GABA α receptor subtype. Flumazenil binds with similar affinity (∼1 nmol/L) to α1, α2, α3, and α5 GABA-benzodiazepine receptors and lower affinity at α4 and α6 subtypes (Sieghart, 1995). Ro15-4513 has 10- to 15-fold higher affinity for the α5 subtype (0.7 nmol/L) compared with all remaining subtypes (Hadingham *et al*, 1993). Conventional compartmental modelling does not, in practical terms, accurately describe the complex pharmacodynamics when multiple receptor subtypes are present, especially when the different subtypes behave differently kinetically and are present in varying ratios depending on the brain region. In this study, compartmental modelling of [11C]Ro15-4513 was not sensitive enough to detect changes in lower-affinity binding to α1 the subtype. Despite the usefulness of these models to show different regional kinetics, they are pharmacological simplifications and not suitable for accurately describing nonselective ligands in quantitative analyses, although a two-tissue compartment model was proposed as effective in all regions by Asai *et al* (2009). Given that no one-compartmental model adequately represented the kinetics of tracer binding in all tissues, and that there are multiple specific binding sites, we suggest this imposes limitations on using the reference region approach for α5-rich regions because it violates its underlying principle that the volume of distribution of nontarget bound ligand is the same in target and reference tissues (Lammertsma and Hume, 1996). The pons is often used as a reference region, given the lack of suitable region devoid of benzodiazepine receptors, but the low binding in the pons is not sufficient to fully meet the assumptions of the reference tissue model. Therefore, binding in regions of interest is underestimated and/or additional steps have to be taken to more accurately estimate such specific binding levels (Litton *et al*, 1994; Klumpers *et al*, 2008; Asai *et al*, 2009).

In this study, spectral analysis consistently yielded higher estimates of V_T relative to compartmental modelling. The whole-brain spectral profiles, using all 83 regions defined in the atlas (Appendix 1; Hammers *et al*, 2007), showed that with both [11C]flumazenil and [11C]Ro15-4513, zolpidem reduced the height of peaks in certain frequency ranges. Subtype differences could not be immediately inferred from these spectral frequency components,

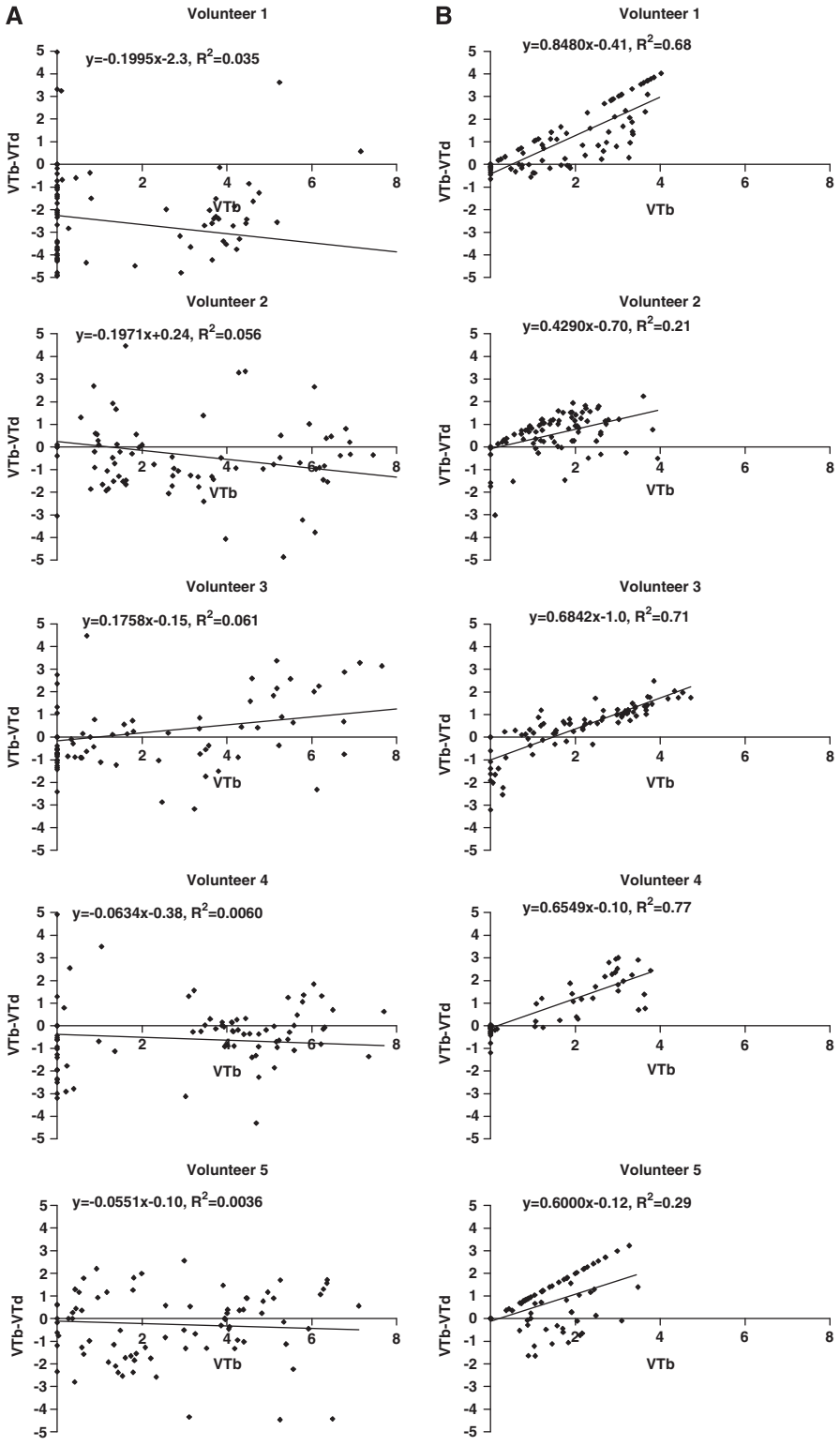

Figure 5 Occupancy plots using the fractional volume of distribution in baseline and postdrug studies, according to equation (2), are shown for each subject. (**A**) Occupancy plots using V_{S1}, defined by the 'slow' peak of the spectral analysis results (summing over $1 \leq k \leq 25$). (**B**) Occupancy plots using $V_{S2,}$ defined by the 'fast' peak (summing over $25 \leq k \leq 50$). Zolpidem occupancy values obtained by linear regression, together with R^2, are shown in each plot. Each data point represents the volume of distribution calculated for each ROI as listed in Appendix 1, excluding the ventricles, known to contain no GABA receptors. ROI, region of interest.

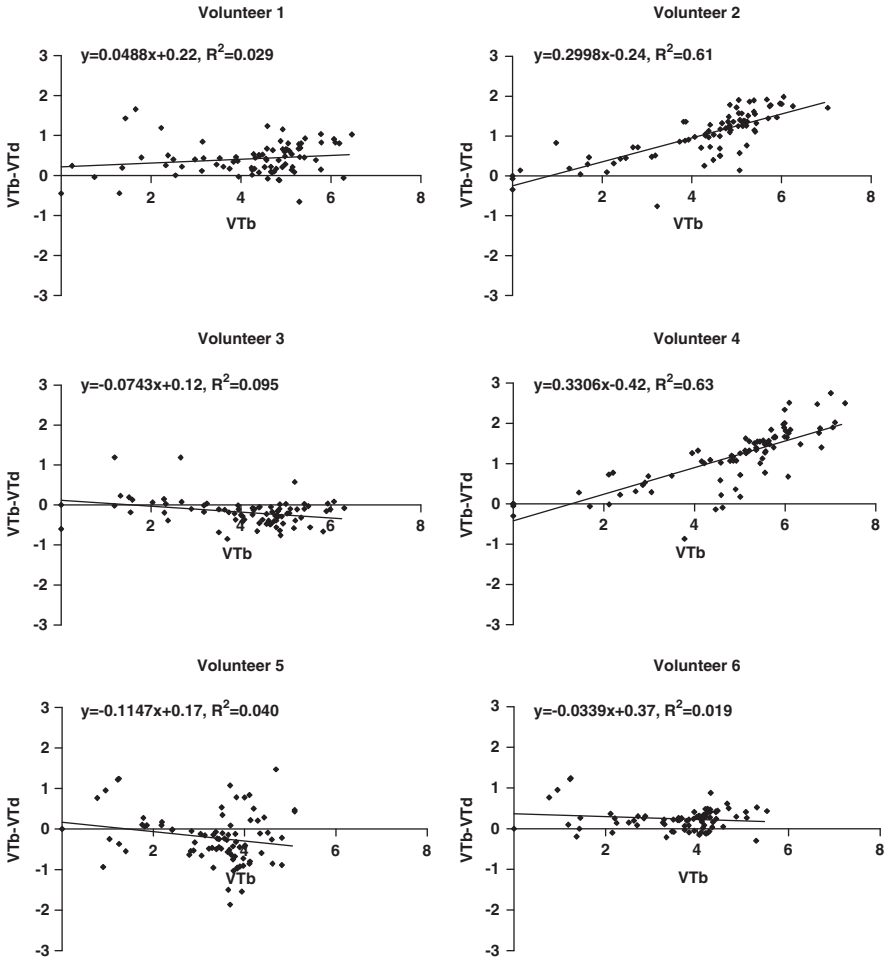

Figure 6 Occupancy plots for the [11C]flumazenil cohort, showing V_T calculated by voxel-wise spectral analysis in each region. Zolpidem occupancy values obtained by linear regression, together with R^2 are shown in each plot. Each data point represents the volume of distribution calculated for each ROI as listed in Appendix 1, excluding the ventricles, known to contain no GABA receptors. ROI, region of interest.

a problem compounded by complexity of the range of subtype ratios in the large number of brain regions included in the analysis. Unfortunately, the spectrum for [11C]flumazenil proved too homogeneous for separation of peaks based on regional receptor subtype density. However, for [11C]Ro15-4513 images, in α5-rich regions such as the hippocampus and nucleus accumbens, we found a high-affinity binding site with a slower kinetic profile, consistent with the fitting of data from these regions with two-tissue compartment models. This slow component was not affected by zolpidem administration, and was therefore attributed to high-affinity binding to the α5 subtype. In addition, in both α5-rich and α5-poor regions, there was a fast kinetic component present that was significantly reduced after zolpidem administration, most likely representing specific binding with lower affinity to the α1 subtype. The intersubject variability of specific volume of distribution defined using these spectral bands was lower than for the total volume of distribution, V_T. Therefore, spectral analysis was shown to be sensitive to detect the contribution of lower-affinity binding of [11C]Ro15-4513 to GABARα1 *in vivo*.

Confirmation of these subtype-specific frequency components in [11C]Ro15-4513 images may be provided with further study using α5-specific blockade. Until that is done, we cannot absolutely exclude that α2 and α3 subtypes may have contributed to the spectra we have taken to represent α5. In addition, there are no drugs selective for α2 and/or α3 available. More broadly, these spectral band-pass methods may be useful to further sharpen analytical tools for *in vivo* PET assays, by reducing noise in the spectrum and by allowing possible subtype-specific probes into other nonselective ligands such as [11C]diprenorphine and [11C]PHNO. Similarly, subtype-specific analyses of [11C]Ro15-4513 PET in clinical and pharmacological applications may yield group effects hitherto overlooked because of the influence of other subtypes on the binding.

Benzodiazepine agonists have previously been believed to exert their effects when occupying only

a relatively small number of receptors in humans. This is based on [11C]flumazenil PET and [123I]iomazenil SPET studies showing sedation or sleep is associated with clonazepam (0.03 mg/kg) at 15% to 23% occupancy, with diazepam (30 mg) at 24%, with alprazolam (2 mg) at 16%, and with midazolam (50 mcg/kg) at 17% to 35% or (6 mg/h) at 20% to 30% (Shinotoh *et al*, 1989; Pauli *et al*, 1991; Videbaek *et al*, 1993; Malizia *et al*, 1996; Fujita *et al*, 1999). Zolpidem is the only licensed benzodiazepine subtype-selective drug with appropriate pharmacokinetics we were able to give to humans though, as it is an agonist, this limited the dose we were able to give safely. Abadie *et al* (1996) reported that 20 mg oral zolpidem resulted in 20% to 29% occupancy of benzodiazepine receptors assessed with [11C]flumazenil PET. We report that using [11C]flumazenil, although occupancy cannot be directly estimated, the relatively small global decreases of ~10% in V_T indicate this apparently low occupancy was made more indeterminate by the signal from receptor subtypes other than α1. Lassen plots confirm that only two volunteers show significant regressions, estimating occupancy of ~30% with $V_{NS} > 1.5$. However, when using the higher frequency component of [11C]Ro15-4513 to estimate V_S at only the presumed α1 site, occupancy estimates ranged from 43% to 85%. This is accompanied by low V_{NS} estimates, < 1 in most volunteers. What contributes to this range is unclear. We are unable to determine whether this was related to plasma levels because only samples from three individuals were available and we only measured one time point and so we have limited pharmacokinetic information. Nevertheless, this higher occupancy is more consistent with that estimated by calculating that a 20 mg tablet given to a 100 kg individual will result in plasma levels of 650 nmol/L. Assuming a volume of distribution in the brain of 0.5% and 90% protein binding, ~130 nmol/L will be available in the brain. As zolpidem has an affinity of ~100 nmol/L at GABARα1 (Hanson *et al*, 2008; Hadingham *et al*, 1993), the administered level of zolpidem should result in high occupancy at this subtype.

It was notable that for both PET ligands, there was high intersubject variability of the effect of zolpidem on ligand binding. This is consistent with report by Abadie *et al* (1996) who also used 20 mg zolpidem with [11C]flumazenil PET and described 'spurious' intersubject variability including increases in [11C]flumazenil binding in the presence of zolpidem as we saw in some of our subjects. Therefore, it seems that subject heterogeneity is commonly seen when investigating the GABA system, of which one consequence has been some studies require large numbers of individuals. It is not clear what contributes to the variability of [11C]flumazenil and [11C]Ro15-4513 binding but because both ligands bind to several different benzodiazepine subtypes, it is possible that relatively small variations in receptor density ratios have a role. For instance, with [11C]Ro15-4513, the greater contribution to binding potential is proposed to come from the high-affinity GABARα5 component, which will be sensitive in ratio to the ubiquitous GABARα1 component. Similarly, it is possible that different subtypes are differentially affected by changes in endogenous GABA levels. It is for this reason that we have developed this technique with [11C]Ro15-4513 to describe the contribution of benzodiazepine receptor subtypes to this variability. This method results in an importantly consistent spread of positive occupancy estimations across all individuals.

We believe this development and application of spectral band-pass methods will help characterise benzodiazepine receptor subtypes as compounds with appropriate relative affinities become available. The use of nonselective ligands to show *in vivo* occupancy of receptor-selective compounds will be more accurate as specific binding of the ligand is estimated. At present, [11C]flumazenil PET has been used to determine occupancy by two such compounds, TPA023 at α2 and α3 and α5IA at α5 (Atack *et al*, 2011). As [11C]flumazenil is nonspecific and α5IA and TPA023 each have equivalent affinity for α1, α2, α3, and α5 subtypes, the reduction in [11C]flumazenil was presumed to reflect occupancy equally at all subtypes to infer occupancy at α2/α3 for TPA023 and α5 for α5IA. Eng *et al* (2010) emphasised the importance of establishing the plasma-occupancy relationship in humans rather than merely relying on preclinical data because in both studies, the EC_{50} in humans was lower compared with preclinical data. Therefore, the approach we have adopted here will greatly enhance our ability to understand the role of different benzodiazepine subtypes and its potential to determine contribution of receptor subtypes in other nonspecific ligands.

Acknowledgements

The authors acknowledge the scan expertise and support provided by Hammersmith Imanet. This paper is dedicated to the memory of Dr Ralph Myers, father, mentor, and friend.

Disclosure/conflict of interest

The authors declare no conflict of interest.

References

Abadie P, Rioux P, Scatton B, Zarifian E, Barré L, Patat A, Baron JC (1996) Central benzodiazepine receptor occupancy by zolpidem in the human brain as assessed by positron emission tomography. *Eur J Pharmacol* 295:35–44

Asai Y, Ikoma Y, Takano A, Maeda J, Toyama H, Fumihiko Yasuno F, Tetsuya Ichimiya T, Ito H, Suhara T (2009)

Quantitative analyses of [11C]Ro15-4513 binding to subunits of GABAA/benzodiazepine receptor in the living human brain. *Nucl Med Commun* 11:872–80

Atack JR, Hallett D, Tye S, Wafford KA, Ryan C, Sanabria-Bohórquez SM, Eng W, Gibson RE, Burns HD, Dawson GR, Carling R, Street L, Pike A, De Lepeleire I, Van Laere K, Bormans G, de Hoon J, Van Hecken A, McKernan R, Murphy M, Hargreaves R (2011) Preclinical and clinical pharmacology of TPA023B, a GABAA receptor alpha2/3 subtype-selective agonist. *J Psychopharmacol* 25:329–44

Barros DAR, Heckemann RA, Rosso L, McGinnity CJ, Keihaninejad S, Gousias IS, Brooks DJ, Duncan JS (2010) Investigating the reproducibility of the novel alpha-5 GABAA receptor PET ligand [11C]Ro15 4513. *8th International Symposium on Functional Neuroreceptor Mapping of the Living Brain* 52:S112

Busatto GF, Pilowsky LS, Costa DC, Ell PJ, David AS, Lucey JV, Kerwin RW (1997) Correlation between reduced *in vivo* benzodiazepine receptor binding and severity of psychotic symptoms in schizophrenia. *Am J Psychiatry* 154:56–63

Cunningham VJ, Jones T (1993) Spectral analysis of dynamic PET studies. *J Cereb Blood Flow Metab* 13:15–23

Cunningham VJ, Rabiner EA, Slifstein M, Laruelle M, Gunn RN (2010) Measuring drug occupancy in the absence of a reference region: the Lassen plot re-visited. *J Cereb Blood Flow Metab* 30:46–50

Defrise M, Kinahan PE, Townsend DW, Michel C, Sibomana M, Newport DF (1997) Exact and approximate rebinning algorithms for 3-D PET data. *IEEE Tran Med Imaging* 16:145–58

Fritschy JM, Möhler H (1995) GABAA-receptor heterogeneity in the adult rat brain: differential regional and cellular distribution of seven major subunits. *J Comp Neurol* 359:154–94

Fujita M, Woods SW, Verhoeff NP, Abi-Dargham A, Baldwin RM, Zoghbi SS, Soares JC, Jatlow PA, Krystal JH, Rajeevan N, Charney DS, Seibyl JP, Innis RB (1999) Changes of benzodiazepine receptors during chronic benzodiazepine administration in humans. *Eur J Pharmacol* 368:161–72

Hadingham KL, Wingrove P, Le Bourdelles B, Palmer KJ, Ragan CI, Whiting PJ (1993) Cloning of cDNA sequences encoding human alpha 2 and alpha 3 gamma-aminobutyric acid A receptor subunits and characterization of the benzodiazepine pharmacology of recombinant alpha 1, alpha 2-, alpha 3-, and alpha 5-containing human gamma-aminobutyric acid A receptors. *Mol Pharmacol* 43:970–5

Hammers A, Chen CH, Lemieux L, Allom R, Vossos S, Free SL, Myers R, Brooks DJ, Duncan JS, Koepp MJ (2007) Statistical neuroanatomy of the human inferior frontal gyrus and probabilistic atlas in a standard stereotaxic space. *Hum Brain Mapp* 28:34–48

Hammers A, Koepp MJ, Labbé C, Brooks DJ, Thom M, Cunningham VJ, Duncan JS (2001) Neocortical abnormalities of [11C]-flumazenil PET in mesial temporal lobe epilepsy. *Neurology* 56:897–906

Hanson SM, Morlock EV, Satyshur KA, Czajkowski C (2008) Structural requirements for eszopiclone and zolpidem binding to the gamma-aminobutyric acid type-A (GABAA) receptor are different. *J Med Chem* 51:7243–52

Klumpers UM, Veltman DJ, Boellaard R, Comans EF, Zuketto C, Yaqub M, Mourik JE, Lubberink M, Hoogendijk WJ, Lammertsma AA (2008) Comparison of plasma input and reference tissue models for analysing [11C]flumazenil studies. *J Cereb Blood Flow Metab* 28:579–87

Lammertsma AA, Hume SP (1996) Simplified reference tissue model for PET receptor studies. *Neuroimage* 4:153–8

Langer SZ, Faure-Halley C, Seeburg P, Graham D, Arbilla S (1992) The selectivity of zolpidem and alpidem for the α1-subunit of the GABAA receptor. *Eur Neuropsychopharmacol* 2:232–4

Lassen NA, Bartenstein PA, Lammertsma AA, Prevett MC, Turton DR, Luthra SK, Osman S, Bloomfield PM, Jones T, Patsalos PN, O'Connell MT, Duncan JS, Andersen JV (1995) Benzodiazepine receptor quantification *in vivo* in humans using [11C]flumazenil and PET: application of the steady-state principle. *J Cereb Blood Flow Metab* 15:152–65

Lingford-Hughes A, Hume SP, Feeney A, Hirani E, Osman S, Cunningham VJ, Pike VW, Brooks DJ, Nutt DJ (2002) Imaging the GABA-benzodiazepine receptor subtype containing the alpha5-subunit *in vivo* with [11C]Ro15 4513 positron emission tomography. *J Cereb Blood Flow Metab* 22:878–89

Lingford-Hughes A, Reid AG, Myers J, Feeney A, Hammers A, Taylor L, Rosso L, Turkheimer F, Brooks DJ, Grasby P, Nutt DJ (2010) A [11C]Ro15 4513 PET study suggests that alcohol dependence in man is associated with reduced {alpha}5 benzodiazepine receptors in limbic regions. *J Psychopharmacol*; E-pub ahead of print 24 September 2010: doi 10.1177/0269881110379509

Lingford-Hughes AR, Wilson SJ, Cunningham VJ, Feeney A, Stevenson B, Brooks DJ, Nutt DJ (2005) GABA-benzodiazepine receptor function in alcohol dependence: a combined 11C-flumazenil PET and pharmacodynamic study. *Psychopharmacology (Berl)* 180:595–606

Litton JE, Hall H, Pauli S (1994) Saturation analysis in PET–analysis of errors due to imperfect reference regions. *J Cereb Blood Flow Metab* 14:358–61

Maeda J, Suhara T, Kawabe K, Okauchi T, Obayashi S, Hojo J, Suzuki K (2003) Visualization of alpha5 subunit of GABAA/benzodiazepine receptor by 11C Ro15-4513 using positron emission tomography. *Synapse* 47:200–8

Malizia AL, Cunningham VJ, Bell CJ, Liddle PF, Jones T, Nutt DJ (1998) Decreased brain GABA(A)-benzodiazepine receptor binding in panic disorder: preliminary results from a quantitative PET study. *Arch Gen Psychiatry* 55:715–20

Malizia AL, Gunn RN, Wilson SJ, Waters SH, Bloomfield PM, Cunningham VJ, Nutt DJ (1996) Benzodiazepine site pharmacokinetic/pharmacodynamic quantification in man: direct measurement of drug occupancy and effects on the human brain *in vivo*. *Neuropharmacology* 35:1483–91

Möhler H, Fritschy JM, Rudolph U (2002) A new benzodiazepine pharmacology. *J Pharmacol Exp Ther* 300:2–8

Nutt DJ, Besson M, Wilson SJ, Dawson GR, Lingford-Hughes AR (2007) Blockade of alcohol's amnestic activity in humans by an alpha5 subtype benzodiazepine receptor inverse agonist. *Neuropharmacology* 7:810–20

Onoe H, Tsukada H, Nishiyama S, Nakanishi S, Inoue O, Langstrom B, Watanabe Y (1996) A subclass of GABAA/benzodiazepine receptor exclusively localized in the limbic system. *Neuroreport* 8:117–22

Pauli S, Farde L, Halldin C, Sedvall G (1991) Occupancy of the central benzodiazepine receptors during benzodiazepine treatment determined by PET. *Eur Neuropsychopharmacol* 1:229–31

Salvà P, Costa J (1995) Clinical pharmacokinetics and pharmacodynamics of zolpidem. Therapeutic implications. *Clin Pharmacokinet* 29:142–53
Sanger DJ (2004) The pharmacology and mechanisms of action of new generation, non-benzodiazepine hypnotic agents. *CNS Drugs* 18:9–15
Shinotoh H, Iyo M, Yamada T, Inoue O, Suzuki K, Itoh T, Fukuda H, Yamasaki T, Tateno Y, Hirayama K (1989) Detection of benzodiazepine receptor occupancy in the human brain by positron emission tomography. *Psychopharmacology (Berl)* 99:202–7
Sieghart W (1995) Structure and pharmacology of gammaaminobutyric acid A receptor subtypes. *Pharmacol Rev* 47:181–234
Spinks TJ, Jones T, Bloomfield PM, Bailey DL, Miller M, Hogg D, Jones WF, Vaigneur K, Reed J, Young J, Newport D, Moyers C, Casey ME, Nutt R (2000) Physical characteristics of the ECAT EXACT3D positron tomograph. *Phys Med Biol* 45:2601–18
Stephens DN, Pistovcakova J, Worthing L, Atack JR, Dawson GR (2005) Role of GABAA alpha5-containing receptors in ethanol reward: the effects of targeted gene deletion, and a selective inverse agonist. *Eur J Pharmacol* 526:240–50
Turkheimer F, Moresco RM, Lucignani G, Sokoloff L, Fazio F, Schmidt K (1994) The use of spectral analysis to determine regional cerebral glucose utilization with positron emission tomography and [18F]fluorodeoxyglucose: theory, implementation, and optimization procedures. *J Cereb Blood Flow Metab* 14: 406–22
Turkheimer FE, Smith CB, Schmidt K (2001) Estimation of the number of 'true' null hypotheses in multivariate analysis of neuroimaging data. *Neuroimage* 13: 920–30
Veronese M, Bertoldo A, Bishu S, Unterman A, Tomasi G, Smith CB, Schmidt KC (2010) A spectral analysis approach for determination of regional rates of cerebral protein synthesis with the L-[1-(11)C]leucine PET method. *J Cereb Blood Flow Metab* 30:1460–76
Videbaek C, Friberg L, Holm S, Wammen S, Foged C, Andersen JV, Dalgaard L, Lassen NA (1993) Benzodiazepine receptor equilibrium constants for flumazenil and midazolam determined in humans with the single photon emission computer tomography tracer [123I]iomazenil. *Eur J Pharmacol* 249:43–51

Appendix 1

Region List

(R = right, L = left)
R hippocampus
L hippocampus
R amygdala
L amygdala
R anterior temporal lobe—medial
L anterior temporal lobe—medial
R anterior temporal lobe—lateral
L anterior temporal lobe—lateral
R parahippocampal and ambient gyri
L parahippocampal and ambient gyri
R superior temporal gyrus
L superior temporal gyrus
R middle and inferior temporal gyri
L middle and inferior temporal gyri
R lateral occipitotemporal gyrus (fusiform gyrus)
L lateral occipitotemporal gyrus (fusiform gyrus)
R cerebellum
L cerebellum
Brainstem
L insula
R insula
L occipital lobe—lateral
R occipital lobe—lateral
L gyrus cinguli—anterior part
R gyrus cinguli—anterior part
L gyrus cinguli—posterior part
R gyrus cinguli—posterior part
L frontal lobe
R frontal lobe
L posterior temporal lobe
R posterior temporal lobe
L parietal lobe
R parietal lobe
L caudate nucleus
R caudate nucleus
L nucleus accumbens
R nucleus accumbens
L putamen
R putamen
L thalamus
R thalamus
L pallidum
R pallidum
Corpus callosum
R lateral ventricle—frontal horn, central part and occipital horn
L lateral ventricle—frontal horn, central part and occipital horn
R lateral ventricle—temporal horn
L lateral ventricle—temporal horn
Third ventricle
L precenntral gyrus—frontal lobe
R precenntral gyrus—frontal lobe
L straight gyrus—frontal lobe
R straight gyrus—frontal lobe
L anterior orbital gyrus—frontal lobe
R anterior orbital gyrus—frontal lobe
L inferior frontal gyrus—frontal lobe
R inferior frontal gyrus—frontal lobe
L superior frontal gyrus—frontal lobe
R superior frontal gyrus—frontal lobe
L postcentral gyrus—parietal lobe
R postcentral gyrus—parietal lobe
L superior parietal gyrus—parietal lobe
R superior parietal gyrus—parietal lobe
L lingual gyrus—occipital lobe

R lingual gyrus—occipital lobe
L cuneus—occipital lobe
R cuneus—occipital lobe
L medial orbital gyrus—frontal lobe
R medial orbital gyrus—frontal lobe
L lateral orbital gyrus—frontal lobe
R lateral orbital gyrus—frontal lobe
L posterior orbital gyrus—frontal lobe
R posterior orbital gyrus—frontal lobe
L substantia nigra
R substantia nigra
L subgenual frontal cortex
R subgenual frontal cortex
L subcallosal area
R subcallosal area
L presubgenual frontal cortex
R presubgenual frontal cortex
L superior temporal gyrus, anterior part
R superior temporal gyrus, anterior part